Astron. Astrophys. 322, 280–290 (1997)

ASTRONOMY
AND
ASTROPHYSICS

Semiregular variables of types SRa and SRb. Silicate dust emission features

Josef Hron, Bernhard Aringer, and Franz Kerschbaum

Institut für Astronomie der Universität Wien, Türkenschanzstraße 17, A-1180 Wien, Austria

Received 6 June 1996 / Accepted 26 November 1996

Abstract. We have analysed the IRAS-LRS spectra of representative samples of O-rich Semiregular (SR) variables of types SRa and SRb and of Mira variables. The silicate features were extracted by fitting the energy distribution with two blackbodies, approximating the continuous emission from the photosphere and the circumstellar dust. The shape and strength of the silicate features in the LRS range were then studied by computing the residual fluxes in 5 selected wavelength regions covering the whole 10 μm and 18 μm features and parts of the 10 μm feature assigned to emission from olivine and possibly corundum. We compare our approach with previous investigations and argue that a quantitative study of details in the feature shape requires subtraction of the stellar and the dust continuum and the use of flux ratios rather than a discrete classification system.

The Miras form an extension of the SRb's towards lower stellar temperatures and higher dust shell opacities and they have slightly higher average dust temperatures. The SRa's seem to be more similar to the Miras in their dust shell properties. The average 10 μm feature shapes of the three groups of variables agree, but taking into account the photospheric and dust shell parameters, systematic differences show up. For stars hotter than about 2900 K, the 10 μm feature width shows a wide range of values but no clear trend with the stellar temperature or the optical depth of the dust shell. These stars are generally SRb variables and have the thinnest dust envelopes. At cooler stellar temperatures, where mostly Miras are found, the optical depth of the dust shell determines the feature width in the sense that thicker shells have narrower features. It appears that the 13 μm feature is obvious only in a narrow range of effective temperature and optical depth of the dust shell.

We discuss our results in terms of radiative transfer effects, differences in the average grain size, annealing and hydration of amorphous silicates and contributions from other dust components. Of these possibilities the last one seems to be most plausible with regard to the behavior of the 10 μm feature width. The observations can be interpreted in terms of changing contributions from olivine and corundum possibly caused by an increasing amount of dust processing (Miras) and the influence of the atmospheric structure on the formation of these dust components (SRb's).

Key words: stars: AGB and post-AGB – stars: circumstellar matter – stars: mass-loss – infrared: stars

1. Introduction

One of the most interesting aspects of circumstellar shells of AGB stars are the properties of the dust grains. The IRAS LRS spectra (IRAS Science Team 1986) provide the most complete and uniform database for investigations of that type (Jourdain de Muizon 1992). Laboratory experiments and theoretical calculations show that the optical depth of the shell, the grain composition, the grain size distribution, the structure of the grains (crystalline or amorphous) and the degree of processing (e.g. annealing) all can affect the shape of the characteristic dust features observed in the LRS wavelength range (Simpson 1991, Ivezić & Elitzur 1995, Borghesi et al. 1985, Nuth & Hecht 1990).

Little-Marenin & Little (1990, LML) studied the LRS spectra of a large sample of O-rich Mira variables. They found a broadening of the silicate feature around 10 μm with decreasing maser activity in the outer parts of the shell, bluer IRAS [12 μm]−[25 μm] colour and decreasing asymmetry in the optical light curve. All these quantities are correlated with the amount of mass loss. LML suggested that the different widths of the silicate features are due to different amounts of amorphous silicates and crystalline olivine. They analysed also a few selected Semiregular (SR) and Irregular variables and noted that for these stars the silicate feature is slightly narrower and shifted to the red compared to Miras. Sloan & Price (1995, SP) analysed the dust emission of more than 500 O-rich AGB variables by introducing a classification system based on various flux ratios. They also found a broadening of the silicate feature with bluer [12 μm]−[25 μm] colour but no significant dependence of the feature shape on the type of stellar variability. Most recently, Sloan et al. (1996) searched for the 13 μm emission feature in the LRS database. They concluded that about half of the AGB

Send offprint requests to: hron@astro.ast.univie.ac.at

stars with oxygen-rich dust show this feature but that its frequency is significantly higher for the SRb variables.

The emission from circum- and interstellar dust consists not only of the well known features but also of a smooth component, generally called continuum (e.g. Millar & Williams 1993). This component mainly reflects the thermal and geometrical properties of the dust while the features contain information about the detailed internal grain structure. The works of LML and SP, although very extensive, both only subtracted a stellar continuum from the observed spectrum. Since the dust continuum is a significant contribution to the observed flux (Ivezić & Elitzur 1995, Kerschbaum & Hron 1996) and since the wavelength dependence of this contribution is quite different from that of the stellar flux, this will especially affect the interpretation of flux ratios in terms of feature shapes. This is even more important when one considers the large range of dust shell properties found for the Semiregulars (Kerschbaum & Hron 1996). In this paper we will therefore present a comparison of the LRS spectra of SR and Mira variables with silicate emission where we isolate the feature emission by removing the contributions from the stellar and the dust continuum.

2. Analysis of the LRS spectra

2.1. The samples

We defined a sample of 55 oxygen-rich SR stars with complete near infrared photometry, high quality fluxes in the IRAS Point Source Catalog (IRAS Science Team 1988) and a 2*n* LRS type (silicate feature). In order to compare objects with different pulsation properties we extended our study to a sample of 27 Mira stars. The selection criteria and the way of analysing the spectra were the same as for the SR variables. Optical data were taken from Kholopov et al. (1985–88, GCVS), the near infrared photometry for the SR variables comes from Kerschbaum & Hron (1994) and Kerschbaum (1995). Near infrared data for the Miras are from Catchpole et al. (1979).

Most of the Miras were already analysed by LML and hence they serve also as comparison objects between our work and theirs. All our Miras and 41 of our SR's are also in the list of SP.

Finally we note that the period distributions of our SR and Mira samples resemble those of the volume limited samples of Kerschbaum & Hron (1992), i.e. our samples can be considered as representative for 2*n* variables.

2.2. Method for analysing the spectra

To extract the feature emission, we approximate the stellar and dust continua for our objects by fitting two blackbodies to the photometric data using the same procedure as described in Kerschbaum & Hron (1996). The resulting fit parameters are the 'photospheric' temperature T_*, a 'dust' temperature $T_{\rm d}$ and the 'size' of the circumstellar shell relative to the star $r = R_d/R_*$. The physical interpretation of these quantities is discussed in the above paper. For the optically thin dust shells of our objects (see below) the superposition of two blackbodies provides an adequate description of the overall energy distribution and the derived parameters can be linked to physical parameters of these stars. Therefore this approach properly takes into account the differences in the photospheric and dust continuum emission between the stars in our sample. We will discuss the uncertainties and advantages of our approach in the following section.

Subsequently, the resulting function was adjusted to the mean flux of the LRS spectra between 8 and 8.6 μm. After the subtraction of this continuum we studied the remaining dust spectra of the stars by measuring and comparing the fluxes in different wavelength ranges. The integrated fluxes are: F_{10} from 8.9 to 14.0 μm (the whole 10 μm silicate feature); F_9 from 8.9 to 10.5 μm (blue wing and maximum of the 10 μm silicate feature); F_{11} from 10.5 to 12.0 μm (red wing and first 'bump' of the 10 μm silicate feature); F_{13} from 12.0 to 14.0 μm (red wing and second 'bump' of the 10 μm silicate feature); F_{18} from 16.0 to 21.0 μm (18 μm silicate feature). The values of F_{10}, F_9/F_{10}, F_{11}/F_{10}, F_{13}/F_{10} and F_{18}/F_{10} for the SR's and the Miras are listed together with the data from the blackbody fits in Tabs. 1 and 2. A few stars showed very weak or peculiar dust features. These objects are marked in the tables and were not included in the analysis. It is interesting to note that three of these objects (VX And, T Cnc and Y Pav) are listed as carbon stars in the GCVS.

In Table 3 we summarize some mean properties of the stars in our sample. [12 μm]–[25 μm] is the zero point corrected IRAS colour, $F_{10}/F_{\rm bol}$ is the ratio of the 10 μm feature strength relative to the bolometric luminosity, $L_{\rm d}/L_*$ is the envelope to stellar luminosity ratio. It is computed from T_*, $T_{\rm d}$ and R_d/R_*. This luminosity ratio is well correlated with the ratio of the dust emission at 60 μm to the bolometric flux (Kerschbaum & Hron 1996), which again is a measure of the flux averaged optical depth of the dust envelope (Ivezić & Elitzur 1995).

The Miras form an extension of the SRb's towards lower T_* and higher $L_{\rm d}/L_*$. The Miras have a slightly higher 'dust' temperature than the SRb's. The significance of this difference is more evident if one compares the histograms of the 'dust' temperatures and it is confirmed from a larger sample of stars with IRAS and near infrared photometry (Kerschbaum, in preparation). There is an overall trend of decreasing T_* with increasing $L_{\rm d}/L_*$ but the scatter in both directions is quite large (typically 400 K and a factor of ten, respectively). The SRa's seem to be intermediate between Miras and SRb's with regard to T_* but more similar to the Miras in their dust shell properties. We will come back to the listed quantities in the following sections.

All the stars in our sample have values of $L_{\rm d}/L_*$ corresponding to dust envelopes which are optically thin in the near IR (Sect. 4.1). This is supported by the fact that the observed energy distributions show two distinguishable components, one from the photosphere and one from the dust. Thus we do not expect a significant effect of circumstellar reddening on the values of T_* and no strong coupling between T_*, $T_{\rm d}$ and $L_{\rm d}/L_*$ due to reddening. The shape of the continuous dust emission (represented here by $T_{\rm d}$) is only determined by the temperature and density structure of the envelope and by the type of dust grains but not by optical depth effects.

Table 1. Blackbody fit parameters and flux ratios for Semiregular variables. Temperatures are in K, F_{10} is in 10^{-10} W m^{-2}. Stars marked with an asterisk have weak or peculiar dust features.

GCVS	IRAS	Var.	m_{bol}	T_*	T_d	$\log(L_d/L_*)$	F_{10}	F_9/F_{10}	F_{11}/F_{10}	F_{13}/F_{10}	F_{18}/F_{10}
ST Psc	01251+1626	SRb	4.71	2536	381	−1.66	0.0151	0.57	0.36	0.07	0.26
SV Psc	01438+1850	SRb	3.63	2511	398	−1.80	0.0217	0.47	0.36	0.17	0.44
W Hor	02427−5430	SRb	3.95	2454	368	−1.32	0.0706	0.35	0.36	0.29	0.25
SU Eri	03489−0131	SRb	3.60	2569	410	−1.82	0.0247	0.50	0.40	0.10	0.22
U Men	04140−8158	SRa	3.26	2115	554	−0.96	0.1270	0.45	0.36	0.19	0.27
RV Cam	04265+5718	SRb	3.48	2582	287	−2.22	0.0109	0.59	0.38	0.02	0.22
RX Lep	05090−1154	SRb	1.61	2784	396	−2.40	0.0428	0.55	0.35	0.10	0.43
FX Ori	05390+1448	SRb	4.64	2761	461	−1.77	0.0160	0.50	0.35	0.15	0.49
S Lep	06036−2411	SRb	2.55	2742	452	−1.74	0.1430	0.49	0.38	0.14	0.26
X CMa	06546−2353	SRb	3.77	2538	390	−1.80	0.0237	0.42	0.38	0.19	0.37
HU Pup	07536−2830	SRa	5.20	2308	370	−0.77	0.0440	0.53	0.37	0.10	0.34
Y Pup	08107−3459	SRb	3.88	2627	405	−2.40	0.0052	0.50	0.44	0.06	0.23
Z Cnc	08196+1509	SRb	4.17	2738	432	−1.85	0.0141	0.53	0.39	0.08	0.32
AK Hya	08375−1707	SRb	2.38	2508	399	−2.00	0.0453	0.44	0.40	0.17	0.37
EP Vel	08400−4755	SRa	4.23	2509	394	−1.43	0.0406	0.47	0.39	0.14	0.30
SY Vel	09105−4334	SRb	3.60	2722	406	−1.92	0.0172	0.60	0.38	0.01	0.30
GM Vel	09457−4624	SRb	4.95	2390	394	−1.85	0.0062	0.43	0.36	0.21	0.53
SZ Vel	09481−4425	SRb	4.01	2685	396	−2.00	0.0096	0.41	0.41	0.18	0.48
VZ Vel	10261−5055	SRa	4.87	2452	443	−1.20	0.0165	0.60	0.30	0.10	0.36
HH Vel	10401−5327	SRb	4.16	2487	391	−1.52	0.0353	0.51	0.37	0.12	0.27
R Crt	10580−1803	SRb	1.85	2177	400	−1.58	0.2690	0.34	0.36	0.30	0.31
RT Vir	13001+0527	SRb	1.93	2170	396	−1.74	0.1646	0.30	0.37	0.33	0.34
V CVn	13172+4547	SRa	3.80	2790	566	−1.42	0.0634	0.61	0.32	0.06	0.20
V744 Cen	13368−4941	SRb	2.28	2834	437	−1.92	0.0510	0.38	0.40	0.21	0.40
θ Aps	14003−7633	SRb	1.01	2699	453	−1.92	0.1381	0.44	0.40	0.17	0.58
RV Boo	14371+3245	SRb	2.97	2840	426	−1.85	0.0274	0.43	0.38	0.18	0.41
RW Boo	14390+3147	SRb	3.43	2946	363	−2.10	0.0093	0.68	0.39	−0.07	0.06
FY Lib	14550−1214	SRb	3.13	2528	389	−2.10	0.0122	0.49	0.41	0.10	0.25
Y Ser	15114−0142	SRa	5.35	2709	493	−1.58	0.0101	0.60	0.36	0.04	0.34
RU CrB	15334+2555	SRa	6.24	2274	511	−1.36	0.0072	0.54	0.34	0.12	0.42
RS CrB	15566+3609	SRa	4.46	2856	506	−1.51	0.0250	0.47	0.37	0.16	0.25
X Her	16011+4722	SRb	1.51	2550	394	−1.89	0.1813	0.52	0.34	0.15	0.24
V988 Oph	18243+0352	SRb	3.78	2700	440	−1.74	0.0356	0.54	0.36	0.10	0.35
RT Pav	18309−6955	SRb	4.32	2734	436	−1.72	0.0173	0.47	0.39	0.15	0.39
SY Lyr	18394+2845	SRb	4.78	2490	297	−1.92	0.0067	0.63	0.34	0.03	0.38
MZ Her	18460+1903	SRb	4.42	2565	312	−2.10	0.0080	0.48	0.34	0.18	0.36
UX Sgr	18520−1635	SRb	3.24	2601	392	−1.92	0.0308	0.53	0.37	0.09	0.40
UV Aql	18562+1417	SRa	4.91	2463	340	−2.05	−0.0034	0.11	0.13	0.76	0.88
V366 Aql	19238+0211	SRa	6.01	1938	380	−1.15	0.0158	0.59	0.33	0.09	0.28
V718 Cyg	20010+3011	SRb	6.23	2065	376	−0.49	0.0288	0.46	0.36	0.18	0.24
X Pav	20075−6005	SRb	1.86	2294	394	−1.62	0.1440	0.37	0.36	0.27	0.07
AI Cyg	20297+3221	SRb	4.44	2855	364	−1.85	0.0052	0.58	0.43	−0.01	0.38
RZ Cyg	20502+4709	SRa	3.90	2000	355	−1.48	0.0531	0.34	0.37	0.29	0.31
RS Cap	21044−1637	SRb	2.71	2651	424	−1.68	0.0959	0.58	0.35	0.07	0.21
EP Aqr	21439−0226	SRb	1.48	2226	420	−1.74	0.2393	0.43	0.33	0.24	0.44
NY Lac	22306+5510	SRb	4.18	2227	340	−1.72	0.0095	0.36	0.40	0.24	0.38
BD Peg	22406+2753	SRb	4.12	2702	301	−2.52	0.0061	0.52	0.33	0.15	0.22
V PsA	22525−2952	SRb	2.49	2373	430	−1.82	0.0445	0.45	0.38	0.17	0.18
BI Peg	22553+1744	SRa	5.28	2334	434	−1.54	0.0129	0.47	0.37	0.15	0.22
AK Peg	23006+1105	SRa	5.81	2727	576	−1.18	0.0205	0.69	0.35	−0.04	−0.02
VX And*	00172+4425	SRa	4.09	2313	328	−2.30	−0.0045	−0.47	0.17	1.30	0.78
RR Eri*	02497−0828	SRb	3.49	3109	423	−2.40	0.0011	1.22	0.70	−0.92	−0.49
T Cnc*	08538+2002	SRb	4.19	2292	418	−1.96	−0.0096	0.10	0.19	0.71	0.62
RW Sgr*	19109−1856	SRa	6.23	2578	550	−1.43	0.0050	0.56	0.28	0.16	0.48
Y Pav*	21197−6956	SRb	3.54	2543	313	−2.15	0.0023	1.41	0.63	−1.04	−1.23

Table 2. Blackbody fit parameters and flux ratios for Miras. Units and symbols as in Table 1.

GCVS	IRAS	Var.	m_{bol}	T_*	T_d	$\log(L_d/L_*)$	F_{10}	F_9/F_{10}	F_{11}/F_{10}	F_{13}/F_{10}	F_{18}/F_{10}
R Cet	02234−0024	M	5.09	2522	384	−1.49	0.0155	0.60	0.32	0.08	0.48
R Hor	02522−5005	M	2.54	2155	486	−1.06	0.1966	0.58	0.36	0.07	0.03
U Ari	03082+1436	M	3.97	2233	437	−1.92	0.0079	0.42	0.37	0.21	0.32
W Eri	04094−2515	M	4.62	2245	529	−1.09	0.0292	0.49	0.34	0.18	0.33
R Tau	04255+1003	M	4.05	2060	446	−1.57	0.0195	0.31	0.37	0.32	0.40
R Cae	04387−3819	M	3.35	2254	517	−1.58	0.0593	0.37	0.36	0.27	0.23
S Pic	05096−4834	M	3.97	2175	489	−1.04	0.0733	0.55	0.34	0.11	0.14
U Dor	05098−6422	M	3.88	2278	392	−1.36	0.0434	0.59	0.33	0.08	0.18
U Pup	07585−1242	M	4.23	2123	453	−1.49	0.0431	0.45	0.36	0.19	0.33
SU Car	10118−6038	M	5.10	2325	412	−1.21	0.0347	0.54	0.35	0.11	0.24
X Cen	11466−4128	M	3.89	2375	476	−1.51	0.0215	0.59	0.34	0.07	0.37
ST Cru	12230−5943	M	3.69	2240	418	−1.49	0.0375	0.44	0.40	0.17	0.16
U Cru	12295−5718	M	4.94	2320	449	−1.26	0.0157	0.55	0.33	0.12	0.26
RU Hya	14086−2839	M	4.90	2335	477	−1.04	0.0238	0.73	0.32	−0.05	0.12
RS Vir	14247+0454	M	4.47	2196	438	−1.09	0.0236	0.69	0.33	−0.01	0.28
Y Lup	14559−5446	M	4.20	2143	425	−1.40	0.0257	0.49	0.34	0.16	0.32
R Nor	15323−4920	M	3.92	2878	389	−1.77	0.0170	0.43	0.37	0.20	0.27
BG Ser	15410−0133	M	3.45	2146	425	−2.05	0.0370	0.30	0.36	0.34	0.34
RT Sco	17001−3651	M	3.94	2073	422	−1.21	0.0188	0.50	0.50	0.00	−0.21
RT Oph	17541+1110	M	5.05	2104	491	−1.12	0.0166	0.35	0.38	0.28	0.19
RR Sgr	19528−2919	M	3.80	2459	595	−1.21	0.0212	0.51	0.37	0.12	0.26
RR Aql	19550−0201	M	3.24	2023	433	−1.26	0.1468	0.61	0.31	0.08	0.22
RU Cap	20296−2151	M	6.09	2192	424	−0.92	0.0151	0.70	0.32	−0.02	0.32
W Aqr	20438−0415	M	4.77	2091	540	−1.35	0.0091	0.33	0.44	0.22	0.21
S Gru	22230−4841	M	3.84	2370	476	−1.41	0.0170	0.51	0.41	0.08	0.10
R Peg	23041+1016	M	3.15	2201	456	−1.77	0.0516	0.38	0.35	0.27	0.28
S Ind*	20526−5431	M	4.56	2524	475	−1.32	0.0016	1.75	1.34	−2.08	−3.71

Table 3. Some properties of the different variability types

Type	n	Period [d]	(J–K)	[12 μm]–[25 μm]	T_* [K]	T_d [K]	$\log(L_d/L_*)$	F_{10}/F_{bol}
SRb	40	162 ± 136	1.40 ± 0.16	0.81 ± 0.18	2570 ± 220	392 ± 43	-1.86 ± 0.33	0.0034 ± 0.0056
SRa	15	310 ± 109	1.54 ± 0.29	0.85 ± 0.31	2420 ± 280	453 ± 89	-1.42 ± 0.38	0.0083 ± 0.0059
Mira	27	374 ± 85	1.50 ± 0.13	0.77 ± 0.20	2260 ± 180	458 ± 49	-1.37 ± 0.28	0.0060 ± 0.0040

2.3. Discussion of the method

To be able to investigate the dependence of the shape of the silicate feature on various properties of the star, the ideal procedure is one which models all the components contributing to the LRS spectrum, i.e. the stellar photosphere, the dust continuum and the feature emission. Such a procedure could be a full 'classical' radiative transfer calculation as done by Simpson (1991) or Ivezić & Elitzur (1995). However, this requires also a number of additional assumptions e.g. on the density law in the dust shell, the grain composition and the dust formation. As the processes responsible for these dust shell properties are far from being completely understood, the assumptions can be treated in different ways (compare e.g. Ivezić & Elitzur 1995 or Windsteig et al. 1996). Windsteig et al. have shown that, in spite of their quite different internal structure, dynamical and 'classical' models are equally successful in reproducing the IRAS colours and dust mass loss rates of carbon stars. The near and mid IR regions are much more sensitive to differences in the envelope strucure because dynamical effects mainly influence the inner regions of the dust shell. Using a 'classical' model thus might lead to conclusions which are based on questionable assumptions. We therefore decided to use blackbody fits to approximate the photospheric and the dust continuum and isolate the feature by subtracting the emission from these blackbodies. This purely empirical approach is not only simple but it also makes the smallest number of assumptions. As a consequence however, only qualitative interpretations can be made. A quantitative interpretation requires better theoretical models. One might argue that our approach introduces also a somehow

artificial separation between the dust continuum and the feature emission which both originate from the same particles. We believe that such a separation is acceptable, because the feature and the continuum represent different properties of the grain and because our dust continuum is defined by the emission from the whole envelope while the feature originates in the inner region of the dust shell. We will now briefly discuss various possible sources of errors of our method.

We did not apply the correction factors to the LRS data as published by Cohen et al. (1992a), since they are generally below 10 % and since these corrections would be the same for all our stars, i.e. they would not introduce any systematic differences.

For approximating the stellar continuum, SP used a modified Planck function where the brightness temperature varies with wavelength (Engelke 1992). For our values of T_* and for the effective temperature chosen by SP, the pure blackbody stellar flux gradients between 8 μm and 20 μm are between 10 % and 20 % smaller than those from the Engelke function. In addition, the contribution from the dust continuum will decrease the effect even further. It is not known, whether this function is also applicable to the highly extended atmospheres of AGB variables. As the total effect is much smaller than the systematic trends found, adopting an Engelke function would not change our results.

A potential source of systematic errors is the assumption that there exists no additional emission or absorption in the chosen fitting interval (8 to 8.6 μm, Sect. 2.2). This may not be correct, since the SiO fundamental band, which can be very strong in cool AGB stars (Cohen et al. 1992b), will cause considerable deviations from the continuum in the area around 8 μm. SP adopted a correction for the effect of this feature. However, it is known that at least in many Mira objects the first overtone bands of the silicon monoxide show intense variations connected to the stellar pulsation (Aringer et al. 1995). Sometimes these bands even disappear completely. Therefore we expect variations also for the fundamental transitions. Thus adopting a constant SiO absorption or neglecting it should both only increase the scatter in the measured fluxes but not introduce strong systematic effects.

Another source of deviations from the real continuum is the dust feature itself, because it can extend below 8.5 μm (Simpson 1991). But the portion of the additional dust emission in the continuum fitting interval should never be large enough to change our results very much. A related point is the blue wavelength limit for F_9 and F_{10} at 8.9 μm. It was chosen to include most of the feature for the majority of stars, F_9/F_{10} and F_{10} vary only by a few percent if this limit is set to 8 μm.

Most of the errors are likely to be caused by a wrong shape of the continuum. This is also the reason why a few of our stars show negative F_{13}/F_{10} values. It turned out that the shape of the blackbody functions in the LRS range is quite sensitive to changes of the photometric input data. As a consequence, also the overall variability of AGB objects would give rise to a scatter of the determined fluxes, especially because the near infrared photometry and the IRAS data were not taken simultaneously. We investigated the possible errors due to the photometric variability by subtracting different simulated continua from the LRS spectra (see also the discussion on the effects of variability in Kerschbaum & Hron 1996). The typical uncertainty of the flux ratios F_9/F_{10}, F_{11}/F_{10} and F_{13}/F_{10} amounts to about ± 0.07, which is much smaller than most of the observed systematic variations of these values. For F_{18}/F_{10} the uncertainty is slightly larger. The uncertainty of F_{10} alone is approximately ± 25 %, which is also small compared to the systematic trend found for the ratio of F_{10} to the bolometric flux (which is much less uncertain).

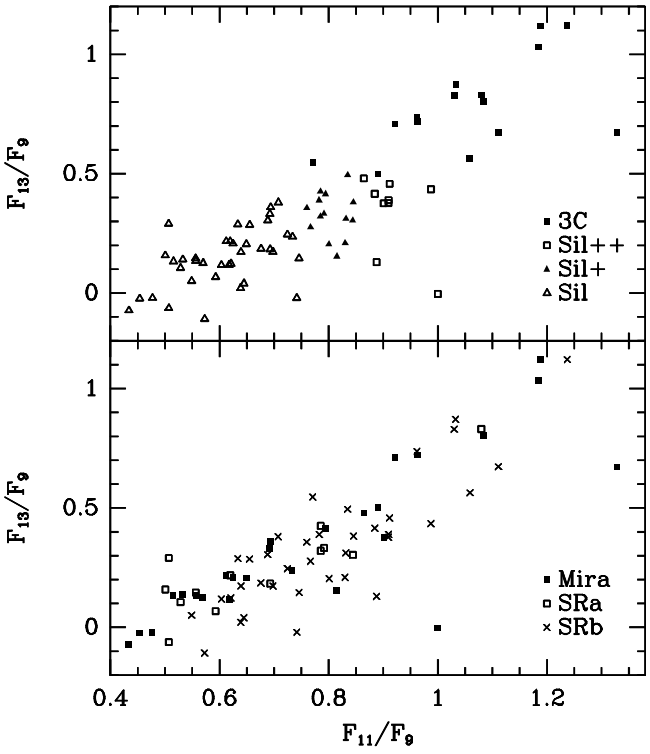

Fig. 1. Flux ratios in the LRS range for the different classes defined by LML (upper) and for the different variability types (lower). See the text for the definition of the ratios.

2.4. Comparison with other methods

As the purpose of this paper is to discuss possible differences between the SR's and the Mira variables, we will concentrate on the works of LML and SP.

After correcting for the continuum emission, we visually classified the 10 μm features in a fashion analog to LML. Since we only included objects of the LRS type 2*n* in our study, we did not cover all the classes defined by LML. We found no S-type features among the SR's, hence we classified the two Miras in our sample with such features as 3C. The existence of the S-features was called into question by SP. In addition, we also found some SR's with no obvious emission feature between 10 and 13 μm among the 2*n* spectra.

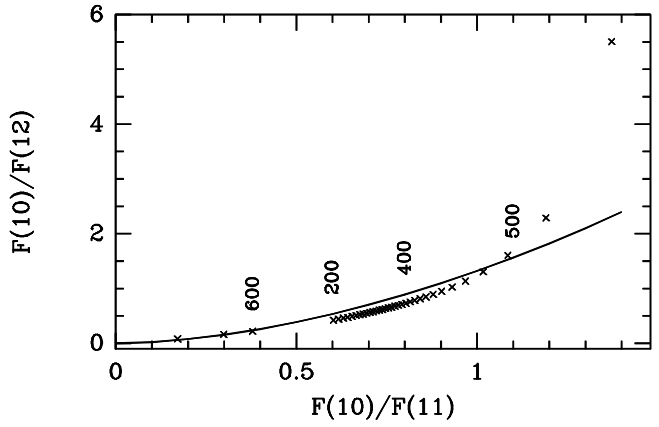

Fig. 2. Comparison of the silicate dust sequence derived by Sloan & Price (1995, full line) and the expected flux ratios at 10, 11 and 12 μm for the sum of two blackbodies when corrected for a 'photospheric' blackbody (see text). Selected 'dust' temperatures are labeled, the spacing is 10 K.

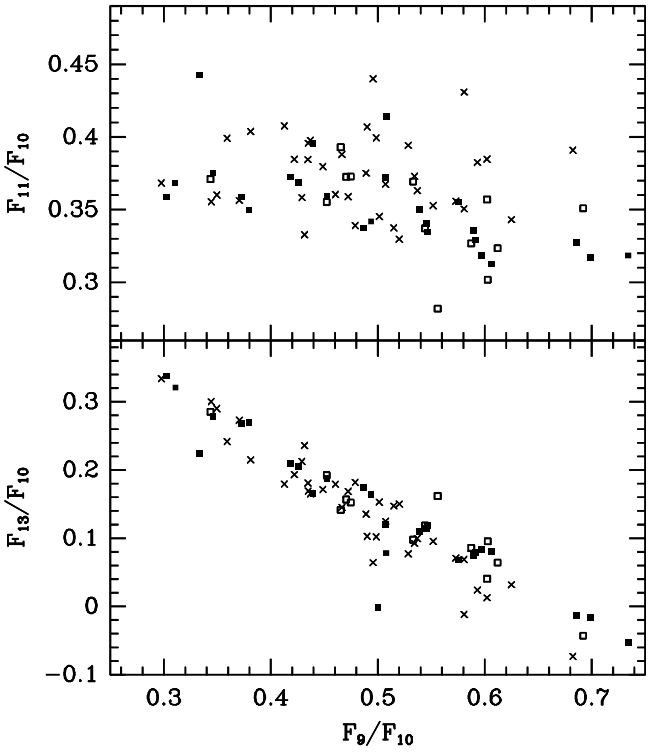

Fig. 3. Various flux ratios in the LRS range (see text) for the different variability types. Symbols for the variables as in Fig. 1.

Since F_9, F_{11} and F_{13} include the emission peaks used in the classification scheme from LML, their classes should be represented by different ratios of these fluxes if the classes are really distinct. Based on the visual classification of the SR spectra and the observed flux ratios, we tried to estimate limiting flux ratios for the various LML classes. In Fig. 1 we show the F_{13}/F_9 and F_{11}/F_9 values for the different classes. These ratios give the best separation between the different LML classes. The corresponding limiting flux ratios for the different classes defined by LML are the following: class Sil, single emission feature with maximum near 10 μm: $F_{11}/F_9 < 0.75$; class Sil$^+$, emission feature with maximum near 10 μm, but with a weak 'bump' around 11.2 μm: $0.75 \leq F_{11}/F_9 \leq 0.85$; class Sil^{++}, emission feature with maximum near 10 μm, but with a strong 'bump' around 11.2 μm: $F_{11}/F_9 > 0.85$; class 3C, feature of three emission peaks around 10, 11 and 13 μm: $F_{13}/F_9 > 0.5$. For the class 3C, we chose F_{13}/F_9 because it allows a better separation than F_{11}/F_9. This is also what we expect from the definition of F_{13}. When using fluxes relative to F_{10}, the separation of the LML classes is not as well defined. However, it is argued below, why we adopt fluxes relative to F_{10} for the analysis of the shape of the 10 μm feature.

By means of the Mira stars in common with LML it was possible to compare our classification with that of LML. In general, the classifications agree but there are some small differences most likely due to inaccuracies by LML in their classification scheme based on visual classification. Thus the disregard of the dust continuum emission by LML had only a small influence on their classification procedure. However, the use of discrete classes reduces the sensitivity for detecting trends between the feature shape and various stellar properties.

The situation is slightly different with regard to the work of SP. They start from flux ratios similar to our scheme but then they introduce also discrete classes (their silicate emission index). Since they do not correct their flux ratios for the contribution of the dust continuum their classification is influenced by the 'dust' temperature. This is illustrated in Fig. 2, which compares the silicate dust sequence of SP (full line) with the flux ratios expected, when a 'photospheric' blackbody of 3000 K is subtracted from the combination of two blackbodies, one with $T_* = 3000$ K and one with a variable 'dust' temperature $T_{\rm d}$. The subtraction was performed in a fashion similar to SP, namely by making the fluxes of the two blackbodies and the 3000 K blackbody agree at 8 μm. With this procedure the relative luminosity of the two blackbodies and the 'stellar' temperature do not enter anymore as parameters. The large variations of the flux ratios corresponding to temperatures between 500 and 600 K are due to the above reduction procedure and the fact that the maximum dust emission (in F_ν) occurs near 10 μm for 500 K. The importance of the 'dust' temperature for the location of a star along the dust sequence is somewhat reduced because each emission index covers flux ratios corresponding to a certain temperature range and because many of our stars have $T_{\rm d}$ below 450 K. Nevertheless, also the scheme of SP is less sensitive than our method for studying the detailed feature shape.

The work of Sloan et al. (1996) should not be affected by the dust continuum because they fitted a polynomial to the silicate feature itself to search for 13 μm emission. We compared our flux ratios for stars with and without this feature according to Sloan et al. but we found only a weak separation. This agrees with the result of Sloan et al. that the 13 μm feature appears for all silicate emission indices, i.e. all LML classes. Since Sloan

et al. really extracted the excess over the silicate emission, they should be more sensitive for the detection of this peak. On the other hand, with their approach they cannot study possible other components in the feature or the overall shape of it. In contrast to Sloan et al., our flux ratios measure the main silicate feature *and* the additional components identified by LML. We will come back to this point in the discussion.

We conclude that for a general classification of the silicate feature, our method is comparable to those of LML and SP but that a quantitative study of details in the feature requires subtraction of the dust continuum and the use of flux ratios rather than a discrete classification system.

3. Results

In this section we will discuss the shape and the strength of the silicate feature at 10 μm as a function of various properties of our stars and the traditional LRS classification (Joint IRAS Science Working Group 1988a). A comparison between Mira and SR variables should show possible effects of stellar pulsation on the behavior of the dust emission. In addition, the intensity of the 18 μm feature will be investigated.

Although fluxes relative to F_9 would give a better separation of the classes defined by LML, we will adopt flux ratios of the form F_i/F_{10} because with such a definition, the trends in F_9 can also be studied and we can separate changes in shape from changes in the total feature strength.

3.1. The position of the 10 μm emission peak

LML noted that the maximum of the silicate feature appears in Miras at shorter wavelengths than in SR stars. This result is confirmed from our much larger SR sample. Miras tend to have their strongest emission peak at 9.7 μm, while its position for most of the SR variables is at 10 μm. This is almost independent of the continuum that has been subtracted from the spectra.

3.2. The shape of the 10 μm Feature

In order to study the shape of the 10 μm feature we measured the portion of the silicate emission in the wavelength ranges 8.9 to 10.5 μm, 10.5 to 12.0 μm and 12.0 to 14.0 μm. The corresponding flux ratios F_9/F_{10}, F_{11}/F_{10} and F_{13}/F_{10} can be found in Table 1. Fig. 3 shows F_{11}/F_{10} and F_{13}/F_{10} as a function of F_9/F_{10} for Mira, SRa and SRb stars. Note that by definition the sum of the three values is always 1. It is remarkable that F_{13}/F_{10} varies much more strongly with F_9/F_{10} than F_{11}/F_{10}. The values range from $F_{13}/F_{10} \sim 0$ for objects with narrow Sil emission to $F_{13}/F_{10} \sim 0.3$ for extreme 3C or broad feature stars. It can already be seen from Fig. 1 that there is little difference in the distribution of the flux ratios between Mira, SRa and SRb variables. The difference in the mean position of the the 10 μm peak apparently does not have any noticable effect, because the ratios are based on fluxes in broader wavelength regions. Since the variations are stronger in F_9/F_{10} and F_{13}/F_{10} than in F_{11}/F_{10}, we will concentrate first on these ratios.

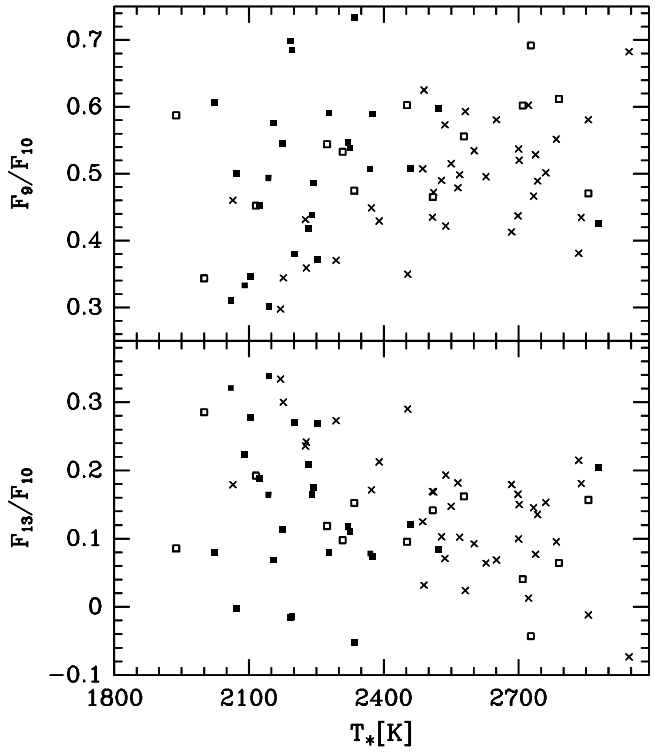

Fig. 4. F_{13}/F_{10} (lower) and F_9/F_{10} (upper) versus the temperature of the 'photospheric' blackbody for Semiregulars and Miras. Symbols as in Fig. 1.

Another interesting result of our study can be seen in Fig. 4, which displays F_9/F_{10} and F_{13}/F_{10} as a function of the 'photospheric' blackbody temperature (T_*). At T_* above about 2400 K, which approximately corresponds to $T_{\rm eff} \gtrsim 2900$ K, the feature width shows no clear trend with temperature. At cooler temperatures, a much wider range of feature widths is found in a narrower range of T_*. It appears as if this behavior holds for both the SR's and the Miras, although there is only a small overlap in the 'photospheric' temperatures of these two groups. The SR's with T_* below 2400 K and broad features are all either 'Mira-like' or 'red' in the notation of Kerschbaum & Hron (1994). If one replaces T_* by the spectral type, one gets similar results, the feature broadening sets in at a spectral type of about M6. This confirms our previous statement that circumstellar reddening does not affect our values for T_*.

As mentioned earlier, the Miras do not only form an extension of the SRb's towards cooler T_* but also towards higher values of L_d/L_*, i.e. higher luminosity contributions from the dust envelope. This luminosity ratio is well correlated with the ratio of the dust emission at 60 μm to the bolometric flux which again is a measure of the flux averaged optical depth of the dust envelope (Sect. 2.2). With respect to $F_\nu(60)/F_{\rm bol}$, the groups of variables show a clearly distinct behavior: For the Miras, the objects with the highest dust luminosities generally have the narrowest features and the features broaden with decreasing $F_\nu(60)/F_{\rm bol}$. The SRb's on the other hand show no clear trend (Fig. 5). Simi-

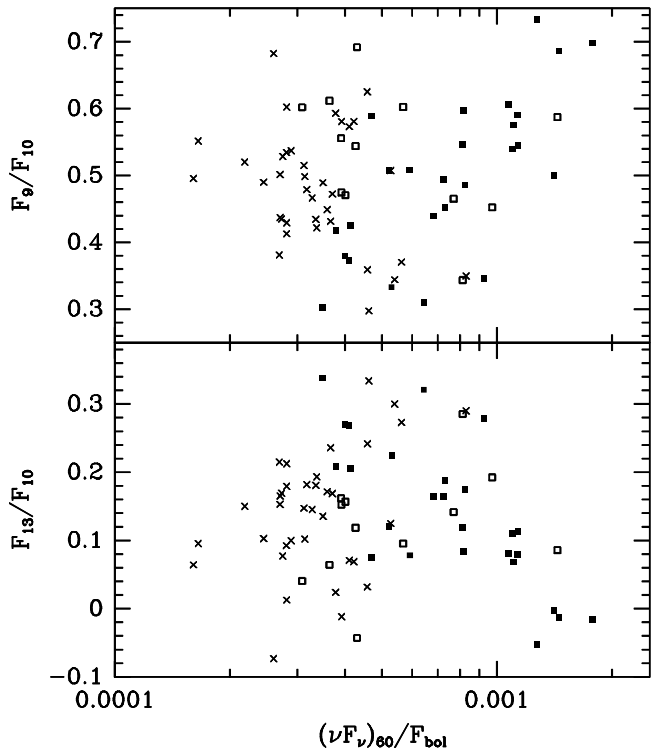

Fig. 5. F_{13}/F_{10} (lower) and F_9/F_{10} (upper) versus the ratio of the 60μm IRAS flux to the total flux. Symbols as in Fig. 1.

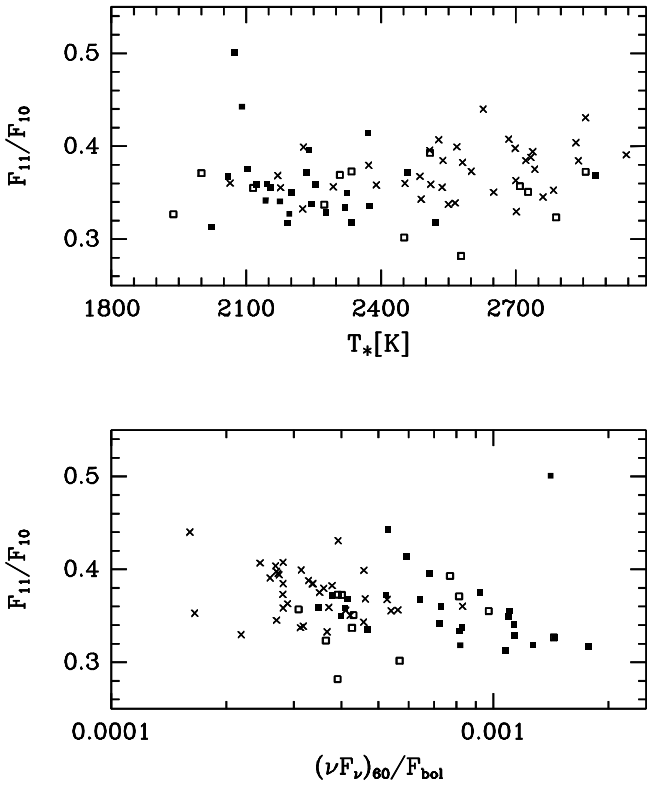

Fig. 6. F_{11}/F_{10} versus T_* (upper diagram) and the ratio of the 60μm IRAS flux to the total flux. Symbols as in Fig. 1.

lar results are found, if one uses (K−12) or L_d/L_* instead of the 60μm flux contribution, again in agreement with a negligible effect of circumstellar reddening on our blackbody fits. This is further supported by the fact that the Miras and SRb's with the narrowest features show the full range of dust shell thickness. The change in the behavior occurs at $F_\nu(60)/F_{bol} \approx 0.0004$ or $L_d/L_* \approx 0.03$. The Miras with the smallest $F_\nu(60)/F_{bol}$ and the SRb's with the largest 60μm flux contribution show comparable values of F_9/F_{10} and F_{13}/F_{10}, i.e. there might be a continuous sequence from SRb's to Miras. The SRb's with the highest 60μm flux contribution are also among the SRb's with the coolest T_*. The SRa's are found both in the Mira and the SRb regions.

The flux ratio F_{11}/F_{10}, which represents a measure for the strength of the 'bump' at 11.2 μm as well as for the width of the central peak of the silicate emission, shows a different behavior: the ratio is larger, i.e. the width is larger, for higher T_* (mostly SR's) and smaller $F_\nu(60)/F_{bol}$ (Fig. 6). However, the magnitude of these two effects is only of the order of the estimated uncertainties.

3.3. The strength of the 10 μm emission

In order to investigate the strength of the dust emission around 10 μm we looked at its contribution to the total bolometric flux of the star (F_{bol}), which can be deduced from the blackbodies that have been fit to the photometry. It should be mentioned at this point that the assumption of a stellar continuum composed of two blackbodies does not affect the resulting bolometric fluxes very much, since any reasonable method of integrating over the photometric data will give similar results.

In Fig. 7 F_{10}/F_{bol} is displayed as a function of L_d/L_*. As one might expect for stars with low to moderate mass loss, the strength of the silicate emission increases with the luminosity of the dust shell blackbody. The Mira variables form an extension of the SRb variables towards higher optical depths and, to a weaker degree, stronger features. One notices that at a constant value of F_{10}/F_{bol}, Miras show a wider spread in the luminosity ratio. This could be explained by the larger bolometric amplitudes of the Miras with respect to the SRb stars, although the distribution of the luminosity ratios at higher feature strengths almost looks bimodal. An alternative explanation could be the wider range of feature widths found for the Miras. At constant optical depth (in our case represented by L_d/L_*) stars with different feature widths can also have different F_{10} values (due to additional dust components, see e.g. Fig. 5 in Ivezić & Elitzur 1995). It seems however unlikely that this can cause differences in the feature strengths of factors of two or more.

If one uses the LRS class as a measure of the feature strength, Miras have a smaller LRS class than SRb variables at the same F_{10}/F_{bol}. This is due to the lower dust luminosity of the SRb's and the definition of the LRS class relative to the local continuum.

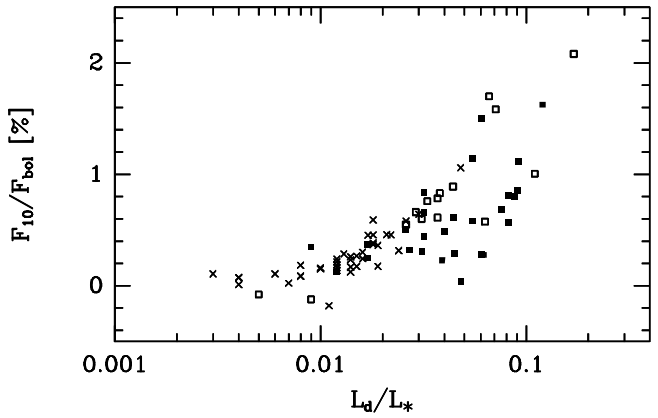

Fig. 7. L_d/L_* versus F_{10}/F_{bol}. Symbols as in Fig. 1.

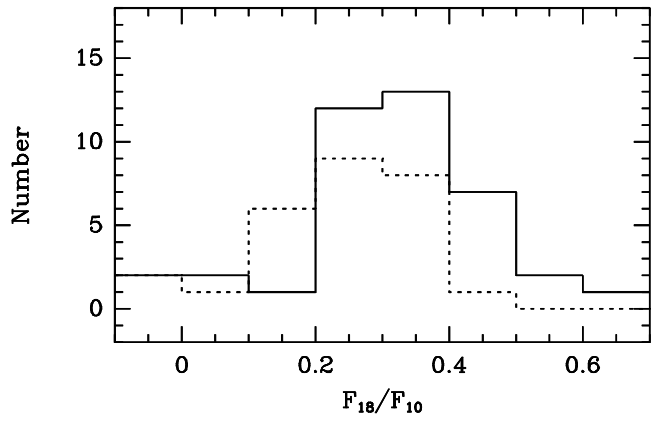

Fig. 8. Histogram of F_{18}/F_{10} for SRb's (full line) and Miras.

3.4. The 18 μm feature

When we analysed the relative strength of the silicate emission around 18 μm (F_{18}/F_{10}), we did not find any obvious correlation of F_{18}/F_{10} with the shape or intensity of the 10 μm feature as well as with the photometric properties of the objects. The SRb variables seem to have slightly higher F_{18}/F_{10} ratios than Miras (Fig. 8), although the difference is statistically only marginally significant.

4. Discussion

First we want to summarize the main results of the previous sections:

- The Miras form an extension of the SRb's towards lower T_* and higher ratios of 'photospheric' to 'dust' luminosity or flux averaged optical depth. The Miras have a slightly higher 'dust' temperature than the SRb's.
- The peak of the 10 μm feature for SR's is shifted by about 0.3 μm towards the red with respect to the Miras.
- The contributions of the 13 μm emission (including the 'bump') and of the blue wing of the 10 μm feature change much stronger with T_* and the dust to star luminosity ratio than that of the 11 μm emission.
- The stars with the broadest features (i.e. largest 13 μm emission and weakest F_9 contribution) have $L_d/L_* \sim 0.03$ and $T_* \lesssim 2200$ K.
- For stars with dust to star luminosity ratios above about 0.03 (mostly Miras and SRa's), the feature width decreases with increasing L_d/L_*. For stars with lower L_d/L_* (mostly SRb's) the feature width shows a wide range of values but no clear trend with L_d/L_* or T_*.
- The small overlap in some of the fit parameters between Miras and SR's does not allow to definitely decide, whether the above trends in the feature width are only defined by L_d/L_* and T_* or if they mainly correspond to different variability types. The behavior of the two groups of variables in the overlap regions of L_d/L_* and T_* seems to support the first hypothesis.
- The total strength of the 10 μm feature increases towards higher values of L_d/L_*.
- SRb's possibly have a slightly higher F_{18}/F_{10} ratio than Miras.
- With respect to the T_* dependence of the feature width and the F_{18}/F_{10} ratio, the SRa's behave intermediately between SRb's and Miras. The L_d/L_* dependence of the feature width and strength are similar to that one of the Miras.

Thus we confirm the results of LML concerning the different peak positions of the silicate feature for Miras and SR's. For Miras, we also agree with LML with regard to the narrowing of the feature with increasing mass loss. Although the average 10 μm feature shapes of the Miras and SR's agree, systematic trends show up when taking into account the differences in the photospheric and dust shell parameters. In this sense we do not confirm the result of SP that there are no systematic differences between the silicate feature shapes of these two groups of variables. Contrary to the results of Sloan et al. (1996), we do not find any difference in the fraction of Miras and SR's with large F_{13}/F_{10}, i.e. with a prominent 13 μm feature. This is not necessarily a contradiction, since our F_{13}/F_{10} ratio measures not only the 13 μm feature and since we have not studied a flux limited sample.

As mentioned in the introduction, a number of parameters can influence the shape and strength of the dust features: the optical depth of the shell, the grain composition, the grain size distribution, the structure of the grains (crystalline or amorphous) and the degree of processing (e.g. annealing). As a starting point of the interpretation we will use the results of radiative transfer calculations which assume a steady mass loss (e.g. Simpson 1991, Ivezić & Elitzur 1995) because dynamical models for stars with oxygen rich dust are not yet available.

4.1. Radiative transfer and particle size effects

From the work of Ivezić & Elitzur, the bolometric fluxes and the 60 μm photometry (or the L_d/L_* values) we can estimate the flux averaged optical depths, τ_f, of the dust shells. Since the optical depth is a global parameter of the shell this estimate should

be qualitatively similar to the result from a dynamical model with the same mass loss rate. For the SRb's the optical depth increases from 0.01 to 0.03 with increasing feature width, while for the Miras τ_f ranges from 0.03 for the stars with the broadest features to about 0.2 for the Miras with the narrowest features. Ivezić & Elitzur have argued that optical depth effects could provide a simple explanation for the different feature shapes. For the Miras, the slight broadening of the feature with decreasing optical depth as well as the corresponding optical depth values would be consistent with such an explanation. However, the behavior of feature widths with optical depth found for the SRb's is not. More important, there is still a marked difference between observed Sil^{++} spectra and those calculated by Ivezić & Elitzur using pure astronomical silicate. Thus optical depth effects alone do not appear sufficient to explain the observed variety of feature shapes, but they may contribute to the observed trend of feature width with optical depth for the Miras.

Particle size effects have been discussed by Simpson (1991). From her work one would expect that a larger mean particle size would mainly affect F_{11}, F_{13} and F_{18}. However, noticable changes in our flux ratios would require differences in the particle sizes of a factor of 7 or more. The dust growth is mainly determined by the density gradient in the shell (Höfner, private communication). Thus we would expect larger particles and broader features for stars with shallower density gradients, i.e. larger pulsation amplitudes (e.g. Bowen 1988). From current dynamical models for dust driven winds in Carbon stars (Höfner & Dorfi 1996), it is unlikely that the required large variations in the particle size can be produced. In addition, many Miras show narrow features and F_{11}/F_{10} also shows the smallest variations of all our flux ratios. Therefore it is unlikely that particle size effects are the dominant factor for the feature shape.

4.2. Additional dust components

The main source for the observed variations in the 10 μm feature shape thus seems to be the influence of additional dust components not contained in pure astronomical silicate. The 'bump' near 11 μm has been tentatively attributed to crystalline olivine (LML, Tielens 1990). The 13 μm 'bump' is generally associated with corundum (Al_2O_3, Dorschner & Henning 1996), although this identification is somewhat uncertain (Sloan et al. 1996). Before trying to interpret our results in terms of different contributions from these materials, one has to remember that our method of analysis cannot isolate the contributions of these components, as it was tried by Sloan et al. for the 13 μm feature. Our flux ratios always contain also the contribution from all other components overlapping in wavelength. We want to mention that due to the resolution of the LRS data, the general broadness of the dust features and the apparently large variations in the feature shape it seems to be very difficult to devise a method which can reliably isolate the individual contributions.

If we restrict the number of dust components to amorphous silicate, olivine and corundum and if we consider the different absorption efficiencies of these three components (e.g. Ivezić & Elitzur 1995 and Sloan et al. 1996), it is likely that F_{11} is a 'blend' of amorphous silicate and olivine. For F_{13}, all three components are of importance. We have used the model spectra of Ivezić & Elitzur computed for a flux averaged optical depth of 0.03, which approximately corresponds to the value for the SRb's, to estimate the change in our flux ratios if 20 % of olivine are included. F_9/F_{10} decreases by about 0.2, F_{11}/F_{10} increases by about 0.07 and F_{13}/F_{10} increases by about 0.15. This demonstrates that the addition of olivine influences also F_{13}/F_{10} and that the flux ratios change in the right direction and by approximately the right amount. Assuming further that the widest features are caused by an additional contribution from corundum makes the observed variations in the flux ratios quite consistent with the values just estimated.

The condensation of crystalline silicates like olivine requires temperatures of the order of 1000 K, the formation of corundum is only possible at even higher temperatures (Tielens 1990). For both components a sufficiently high particle density is necessary, making the formation of olivine more likely in more extended atmospheres. According to Tielens, corundum can be converted into Ca,Al–silicates onto which olivine can form at lower temperatures. At even lower temperatures the amorphous silicates will then be produced. Qualitatively this agrees also with the calculations of Dominik et al. (1993) although Al_2O_3 was not included in these calculations and the condensation temperatures are quite different. Our results indicate that there is apparently only a small temperature and density regime where corundum shows an obvious feature at 13 μm. The decreasing contribution from olivine and corundum found for the stars with $L_d/L_* \gtrsim 0.03$ (mostly Miras) could be due to an increasingly efficient conversion of these dust components into amorphous silicate. This increased efficiency would come not only from the generally denser envelopes but perhaps also from stronger shock fronts which are accompanied by denser and cooler post-shock regions. The total effect on the feature width could be enhanced by the optical depth and particle size effects discussed above.

The lack of correlation between feature width, effective temperature and dust shell thickness for the hotter stars with the thinnest envelopes (mostly SRb's) makes an interpretation quite difficult. Apparently the atmospheric conditions are not very favorable for the formation of olivine and corundum. The higher effective temperatures and the weaker shock fronts of SRb's are likely reasons, the lower 'dust' temperatures could be further evidence. The SRb's are probably in a transition region between static and dynamical atmospheres and in view of the strong and non-linear interplay between dust, gas and pulsations (e.g. Fleischer et al. 1991) a complex behavior of the dust formation process is to be expected.

4.3. The 18 μm feature and the 10 μm peak position

If the Miras really have a slightly lower F_{18}/F_{10} ratio, the optical depth of the shell is not a likely explanation because one would expect no change of this ratio with increasing optical depth for optically thin envelopes (Ivezić & Elitzur 1995). Annealing or hydration in the hotter and denser inner dust envelopes of Miras would cause a *higher* ratio (Nuth & Hecht 1990). On the other

hand, Rowan-Robinson & Harris (1982) found a decrease of the flux ratio for an increase in the temperature of the hottest grains which would be consistent with the slightly higher $T_{\rm d}$ of the Miras.

The slightly longer wavelength of the silicate peak in SR variables as compared to Miras could be due to a larger degree of annealing of the grains in SR's (Nuth & Hecht 1990). As discussed above, the effects of annealing are not in agreement with the possibly larger F_{18}/F_{10} ratio of the SR's. Larger particles would also shift the peak to longer wavelengths (Simpson 1991) but the thinner dust shells and the weaker shock fronts in SR's are not in favor of a more efficient grain growth. A more likely explanation for this subtle difference between Miras and SR's are optical depth effects.

5. Summary and conclusions

We have performed a detailed comparison of the silicate features in Miras and Semiregulars. To extract the features, we have fitted the observed energy distribution with two blackbodies, one for the photospheric and one for the dust continuum. We have chosen this empirical approach because it involves the smallest number of assumptions on the dust formation process and the structure of the dust envelope.

For stars hotter than about 2900 K, the 10 μm feature width shows a wide range of values but no clear trend with the stellar temperature or the optical depth of the dust shell. These stars are generally SRb variables and have the thinnest dust envelopes. At cooler stellar temperatures, where mostly Miras are found, the optical depth of the dust shell determines the feature width in the sense that thicker shells have narrower features. It appears that the 13 μm feature is obvious only in a narrow range of effective temperature and optical depth of the dust shell. The observations can be understood in terms of different contributions from olivine and corundum. For the Miras this is possibly caused by an increasing amount of dust processing while for the SRb's the higher effective temperatures and weaker shock fronts of these stars might be the reason. Slight differences between Semiregular and Mira variables in the peak position of the 10 μm feature and the strength of the 18 μm feature could be due to optical depth effects and the higher dust temperature of the Miras.

Both the process of dust formation in AGB stars and the atmospheric structure of these variables require complex model calculations. For C-rich stars such models are becoming available (e.g. Höfner & Dorfi 1996) and they have been combined with detailed radiative transfer calculations (Windsteig et al. 1996). Unfortunately, the situation is much less favorable in the case of O-rich chemistry. However, the qualitative results from C-rich stars for the atmospheric structure and the results for O-rich dust formation in stationary outflows (Dominik et al. 1993) could be combined with radiative transfer models to yield more realistic dust spectra. In addition, the ISO mission and ground based spectroscopy in the mid infrared will also provide a large set of data of higher resolution than the IRAS-LRS. This should allow a check of the results obtained in this paper and improve our understanding of the formation of dust in O-rich AGB stars.

Acknowledgements. We would like to thank Dr. Susanne Höfner for enlightening discussions on the dynamics of dusty AGB star atmospheres and the referee, Dr. Irene Little-Marenin, for her constructive criticism. Dr. G. Sloan is acknowledged for providing us with his list of silicate emission indices and for his comments on an earlier version of this paper. Mag. Walter Windsteig kindly computed some test spectra for C-stars. BA received a research grant from the University of Vienna. This work was supported by the *Fonds zur Förderung der wissenschaftlichen Forschung* under project numbers P9638-TEC/AST and S7308-AST.

References

Aringer B., Wiedemann G., Käufl H.U., Hron J., 1995, Ap&SS 224, 421
Borghesi A., Bussoletti E., Colangeli L., De Blasi C., 1985, A&A 153, 1
Bowen G.W., 1988, ApJ 329, 299
Catchpole R.M., Robertson B.S.C., Lloyd Evans T.H.H., et al. 1979, SAAO Circulars 1, 61
Cohen M., Walker R.G. Witteborn F.C., 1992a, AJ 104, 2030
Cohen M., Witteborn F. C., Carbon D. F., et al., 1992b, AJ 104, 2045
Dominik C., Sedlmayr E., Gail H.-P., 1993, A&A 277, 578
Dorschner J. Henning, Th. 1996, A&AR, in press
Engelke C.W., 1992, AJ 104, 1248
Fleischer A.J., Gauger A., Sedlmayr E., 1991, A&A 242, L1
Höfner, S., Dorfi, E.A., 1996, A&A, in press
Ivezić Ž, Elitzur M., 1995, ApJ 445, 415
IRAS Science Team 1986, A&ASS 65, 607 (IRAS-LRS)
IRAS Science Team 1988, IRAS Catalogs and Atlases, Volumes 2–6, NASA RP–1190 (IRAS-PSC)
Jourdain de Muizon M., 1992, The IRAS-LRS Database. In: Encrenaz Th. Kessler M.F. (eds.) Les Houches Summer School 1992, Infrared Astronomy with ISO, Nova Science Publ., p. 489
Kerschbaum F., Hron J., 1992, A&A 263, 97
Kerschbaum F., Hron J., 1994, A&AS 106, 397
Kerschbaum F., 1995, A&AS 113, 441
Kerschbaum F., Hron J., 1996, A&A 308, 489
Kholopov P.N. et al. 1985–88, Gen. Cat. of Var. Stars, 4^{th} edition, Nauka Publ. House, Moscow (GCVS)
Little-Marenin I.R., Little S.J., 1990, AJ 99, 1173 (LML)
Millar T.J., Williams D.A., 1993, Dust and Astrochemistry. In: Millar T.J., Williams D.A. (eds.) Dust and chemistry in astronomy, The Graduate Series in Astronomy, Institute of Physics Publishing, Bristol, p. 1
Nuth J.A., Hecht, J.H. 1990, Ap&SS 163, 79
Rowan-Robinson M., Harris S., 1982, MNRAS 200, 197
Simpson J.P., 1991, ApJ 368, 570
Sloan G.C., Price S.D., 1995, ApJ 451, 758 (SP)
Sloan G.C., Le Van P.D., Little-Marnin I.R., 1996, ApJ 463, 310
Tielens A.G.G.M., 1990, Towards a Circumstellar Silicate Mineralogy. In: Mennessier M.O., Omont A. (eds.) From Miras to Planetary Nebulae, Editions Frontiéres, Gif sur Yvette, p. 186
Windsteig W., Dorfi E.A., Höfner S., Hron J., Kerschbaum F., 1996, A&A, in press

This article was processed by the author using Springer-Verlag LaTeX A&A style file *L-AA* version 3.